

Article

Structural Chemistry of Halide including Thallides $A_8Tl_{11}X_{1-n}$ ($A = K, Rb, Cs$; $X = Cl, Br$; $n = 0.1-0.9$)

Stefanie Gärtner ^{1,2,*} , Susanne Tiefenthaler ¹, Nikolaus Korber ¹ , Sabine Stempfhuber ² and Birgit Hischa ²

¹ Institute of Inorganic Chemistry, University of Regensburg, 93040 Regensburg, Germany; Susanne.tiefenthaler@ur.de (S.T.); Nikolaus.korber@ur.de (N.K.)

² Central Analytics, X-ray Crystallography Dept., University of Regensburg, 93040 Regensburg, Germany; sabine.stempfhuber@ur.de (S.S.); Birgit.hischa@ur.de (B.H.)

* Correspondence: Stefanie.gaertner@ur.de; Tel.: +49-941-943-4446

Received: 23 July 2018; Accepted: 7 August 2018; Published: 10 August 2018



Abstract: A_8Tl_{11} ($A =$ alkali metal) compounds have been known since the investigations of Corbett et al. in 1995 and are still a matter of current discussions as the compound includes one extra electron referred to the charge of the Tl_{11}^{7-} cluster. Attempts to substitute this additional electron by incorporation of a halide atom succeeded in the preparation of single crystals for the lightest triel homologue of the group, $Cs_8Ga_{11}Cl$, and powder diffraction experiments for the heavier homologues also suggested the formation of analogous compounds. However, X-Ray single crystal studies on $A_8Tl_{11}X$ to prove this substitution and to provide a deeper insight into the influence on the thallide substructure have not yet been performed, probably due to severe absorption combined with air and moisture sensitivity for this class of compounds. Here, we present single crystal X-Ray structure analyses of the new compounds $Cs_8Tl_{11}Cl_{0.8}$, $Cs_8Tl_{11}Br_{0.9}$, $Cs_5Rb_3Tl_{11}Cl_{0.5}$, $Cs_{5.7}K_{2.3}Tl_{11}Cl_{0.6}$ and $K_4Rb_4Tl_{11}Cl_{0.1}$. It is shown that a (partial) incorporation of halide can also be indirectly determined by examination of the Tl-Tl distances, thereby the newly introduced cdd/cd_{av} ratio allows to evaluate the degree of distortion of Tl_{11}^{7-} clusters.

Keywords: thallide; intermetallics; single crystal; X-ray structure analysis

1. Introduction

Naked cluster anions of the main group elements are well-known for group 14 and 15 elements in solid-state [1–4]. Most of these compounds can be described in terms of the Zintl-Klemm concept [5–7] by formally transferring the valence electrons of the electropositive element to the electronegative under formation of salt-like structures, so called polyanionic salts. Homoatomic group 14 or 15 element polyanions are known since Zintl himself in 1930 stated the existence of Pb_9^{4-} during potentiometric titrations in liquid ammonia solutions [5]. In contrast, the existence of naked group 13 element clusters is not self-evident due to lower values for the electron affinity of group 13 elements which results in a predominantly metallic character of the analogous compounds [3,8]. The first naked thallium cluster was described in 1967 by Hansen and Smith in the binary solid-state compound Na_2Tl [9], which contains Tl_4 tetrahedra with a calculated formal charge of -8 by assuming complete electron transfer. These tetrahedral assemblies are related to the structures of ATt (A : alkali metal, Tt : group 14 element) [10–12] and white phosphorus due to their formal iso-(valence)-electronic character. The largest (empty) thallide cluster is represented by the Tl_{11}^{7-} cluster which is present in binary materials A_8Tl_{11} [13,14] and $A_{15}Tl_{27}$ [15] ($A = K, Rb, Cs$). The A_8Tr_{11} ($Tr =$ group 13 element) structure type was first described in 1991 for the lighter homologue indium in K_8In_{11} [16], of which the crystal structure proved the presence of a naked, pentacapped trigonal prismatic shaped In_{11} cluster, which was

assigned a charge of -7 . Additionally, one extra-electron per formula unit is present, being responsible for the metallic character. The additional electron, referred to the charge of -7 of the cluster anion, is not necessary for the stability of the clusters [17] and can be replaced by halide atoms, which are located on a -3 void (Wyckoff position $6b$) at the origin of the unit cell resulting in a diamagnetic character of the compounds. Halide incorporation was proven for the lighter homologue of the group, $\text{Cs}_8\text{Ga}_{11}\text{Cl}$ by X-ray single crystal structure analysis [18]. Powder diffraction experiments suggested the formation of the heavier homologues $\text{Rb}_8\text{Ga}_{11}\text{Cl}$, $\text{Cs}_8\text{Ga}_{11}\text{X}$ ($\text{X} = \text{Br}, \text{I}$), $\text{Rb}_8\text{In}_{11}\text{Cl}$, $\text{Cs}_8\text{In}_{11}\text{Cl}$, $\text{Cs}_8\text{Tl}_{11}\text{X}$ ($\text{X} = \text{Cl}, \text{Br}, \text{I}$). Recently, continuative studies on halides A_8Tr_{11} ($\text{Tr} = \text{Ga}, \text{In}$) have been reported [19]. However, the formation of $\text{Rb}_8\text{Tl}_{11}\text{Cl}$ was termed as doubtful due to the lack of a significant change in the lattice constants compared to the binary phase $\text{Rb}_8\text{Tl}_{11}$, which also is a common problem for the remaining halide including thallides of this structure family. Therefore, well-resolved single crystal X-ray diffraction studies should provide a deeper insight into the involvement and the role of halide in $\text{A}_8\text{Tl}_{11}\text{X}$ compounds. Thereby, we concentrated on the heavier alkali metals K, Rb and Cs as for sodium no experimental evidence of Tl_{11} clusters is reported.

The questions we wanted to answer were: (1) How does the geometry of the thallide cluster change on halide incorporation; (2) Is there a $\text{Rb}_8\text{Tl}_{11}\text{Cl}$? (3) How do mixed cation sites affect the amount of halide incorporation?

In Section 3 (Results), we report on the first single crystal X-Ray structure determination of halide including thallides, $\text{Cs}_8\text{Tl}_{11}\text{Cl}_{0.8}$, $\text{Cs}_8\text{Tl}_{11}\text{Br}_{0.9}$, $\text{Cs}_5\text{Rb}_3\text{Tl}_{11}\text{Cl}_{0.5}$, $\text{Cs}_{5.7}\text{K}_{2.3}\text{Tl}_{11}\text{Cl}_{0.6}$ and $\text{K}_{3.98}\text{Rb}_{4.02}\text{Tl}_{11}\text{Cl}_{0.1}$. Subsequently, (Section 4, Discussions), the crystal structures are investigated according to the questions listed above.

2. Materials and Methods

All compounds have been synthesized via a stoichiometric approach using high temperature solid state techniques. Cesium and rubidium were produced by the reduction of the corresponding alkali metal halide with elemental calcium [20] and distilled twice, potassium was segregated for purification. Thallium lumps have been stored under inert atmosphere and were used without further purification. The starting materials were enclosed in tantalum crucibles (for stoichiometric approaches see Appendix A) which were subsequently placed in quartz glass ampoules and sealed under argon atmosphere. The same temperature program was used for all compounds: Heating to $700\text{ }^\circ\text{C}$ with a heating rate of $50\text{ }^\circ\text{C}/\text{h}$, holding for 24 h, cooling to room temperature with a cooling rate of $3\text{ }^\circ\text{C}/\text{h}$ to allow for crystallization.

All compounds are very sensitive towards moisture and oxygen and degeneration of the crystals was observed (gassing) in dried mineral oil within few hours. Suitable single crystals for X-ray structure analysis were isolated in dried mineral oil and mounted on a Rigaku SuperNova (Rigaku Polska Sp. Z o. o. Ul, Wroclaw, Poland) (Mo-source, Eos detector) using MiTeGen loops. Thereby, the transfer needed to be very quick as the crystals started to decompose as soon as the mineral oil film became too thin. Once being placed on the diffractometer in the nitrogen stream at 123 K the crystals remained stable and data collection was possible.

Powder diffraction samples were measured in sealed capillaries (0.3–0.5 mm) on a Powder on a STOE Stadi P diffractometer (STOE, Darmstadt, Germany) (monochromatic $\text{Mo-K}_{\alpha 1}$ radiation $\lambda = 0.70926\text{ \AA}$) equipped with a Dectris Mythen 1 K detector.

3. Results

All compounds crystallize in the K_8In_{11} structure type (rhombohedral, spacegroup $R\bar{3}c$) and especially for the mixed alkali metal compounds many of the crystals happened to form typical “multicrystals”. Due to the presence of reverse/obverse twinning a $R(\text{obv})$ filter was applied during data reduction [21]. The materials naturally possess very high absorption coefficients ($\mu > 60\text{ mm}^{-1}$), therefore small single crystals have been chosen for the X-ray analyses. However, the data sets

still suffer from severe absorption effects which could be reduced by carefully applying numerical absorption correction [21]. Thereby, the adjustment of the correct shape played a dominant role.

Table 1 lists the data for the structure determination. For the chloride including compounds two additional, unresolved but several times reproduced residual electron density peaks ($\approx 1.5 \text{ \AA}$ beside the chlorine atom, $\approx 2.2 \text{ \AA}$ beside cesium; along the *c*-axis) are present, which we attribute to unresolved absorption effects as this direction is along the thinnest direction of the plate like crystals. For the bromine including compound this effect is not as dominant as for the chlorine including ones but still is observed.

Table 1. Crystal data and structure refinement details.

Compound	Cs ₈ Tl ₁₁ Cl _{0.80}	Cs ₈ Tl ₁₁ Br _{0.92}	Cs _{5.13} Rb _{2.87} Tl ₁₁ Cl _{0.49}	Cs _{5.67} K _{2.33} Tl ₁₁ Cl _{0.60}	K _{3.98} Rb _{4.02} Tl ₁₁ Cl _{0.1}
CSD number *	434541	434540	434539	434538	1856564
Mr [g·mol ⁻¹]	3339.71	3385.20	3192.52	3114.02	2751.04
Crystal system	Trigonal	Trigonal	Trigonal	Trigonal	Trigonal
Space group	R-3c	R-3c	R-3c	R-3c	R-3c
<i>a</i> [Å]	10.4691 (4)	10.5608 (3)	10.3791 (5)	10.3291 (9)	10.0948 (4)
<i>b</i> [Å]	10.4691 (4)	10.5608 (3)	10.3791 (5)	10.3291 (9)	10.0948 (4)
<i>c</i> [Å]	53.297 (3)	53.401(2)	52.437 (3)	51.909 (5)	51.0274 (18)
α [°]	90	90	90	90	90
β [°]	90	90	90	90	90
γ [°]	120	120	120	120	120
<i>V</i> [Å ³]	5058.8 (5)	5157.9 (4)	4892.0 (5)	4796.3 (9)	4503.3 (4)
<i>Z</i>	6	6	6	6	6
<i>F</i> (000)	8068.0	8180.0	7726.0	7544.0	6703.0
ρ_{calc} [g·cm ⁻³]	6.578	6.539	6.502	6.469	6.087
μ [mm ⁻¹]	60.902	60.745	64.052	61.908	65.822
2 θ -range for data collection [°]	7.59 to 58.982	7.558 to 69.266	7.694 to 54.202	7.758 to 54.198	7.91 to 69.18
Reflections collected/independent	79177/1473	12097/2374	3174/1194	3394/1176	5040/1934
Data/restraints/parameters	1473/0/36	2374/0/36	1194/0/34	1176/0/34	1934/1/37
Goodness-of-fit on <i>F</i> ²	1.244	1.136	1.089	1.148	1.033
Final <i>R</i> indices [<i>I</i> > 2 σ (<i>I</i>)]	<i>R</i> 1 = 0.0280 <i>wR</i> 2 = 0.0619	<i>R</i> 1 = 0.0242 <i>wR</i> 2 = 0.0528	<i>R</i> 1 = 0.0392 <i>wR</i> 2 = 0.0928	<i>R</i> 1 = 0.0456 <i>wR</i> 2 = 0.0996	<i>R</i> 1 = 0.0242 <i>wR</i> 2 = 0.0461
<i>R</i> indices (all data)	<i>R</i> 1 = 0.0309 <i>wR</i> 2 = 0.0629	<i>R</i> 1 = 0.0280 <i>wR</i> 2 = 0.0541	<i>R</i> 1 = 0.0466 <i>wR</i> 2 = 0.0970	<i>R</i> 1 = 0.0566 <i>wR</i> 2 = 0.1034	<i>R</i> 1 = 0.0292 <i>wR</i> 2 = 0.0478
<i>R</i> _{int}	0.0497	0.0385	0.0446	0.0449	0.0280
Largest diff. peak/hole [e·Å ⁻³]	2.96/−1.38	1.83/−3.38	4.82/−2.29	3.62/−2.21	1.48/−1.67

* Further details of the crystal structure investigation(s) may be obtained from The Cambridge Crystallographic data centre CCDC on quoting the deposition number CSD-xxxxxx or the the deposition number CCDC-xxxxxx at <https://www.ccdc.cam.ac.uk/structures/>

With only cesium being present in Cs₈Tl₁₁Cl_{0.8} and Cs₈Tl₁₁Br_{0.9} we obtained phase pure materials according to the powder diffraction pattern of the bulk material (Figure 1; refined cell constants at room temperature: Cs₈Tl₁₁Cl_{0.8}: *a* = 10.566 (5) Å, *c* = 53.67 (3) Å, R-3c; Cs₈Tl₁₁Br_{0.9}: *a* = 10.613 (3) Å, *c* = 53.680 (19) Å).

The well-crystallized Cs₈Tl₁₁X crystals and the resulting good quality single crystal diffraction data allowed the splitting of one alkali metal position according to the site occupancy factor (s.o.f.) of the halide atom (see Section 4.3).

For the mixed alkali metal compounds, we always additionally observed less reduced A₁₅Tl₂₇ phases as a side product. This observation became reasonable when we determined the N_E value (number of electrons per thallium atom) which sums up to a value of 8/11 = 0.72 for A₈Tl₁₁, 15/27 = 0.55 for A₁₅Tl₂₇ and 7/11 = 0.63 for A₈Tl₁₁X. The formation of less reduced A₁₅Tl₂₇ were completely comprehensible if the higher reduced A₈Tl₁₁X_x (*x* << 1) phases would have formed when the halide content was significantly less than 1, because the overall degree of reduction was given by the stoichiometric approach for A₈Tl₁₁X. If less halide was incorporated, this is according to a higher degree of reduction and consequently, a less reduced phase was formed in addition. The remaining halide re-crystallized as (mixed) AX, of which we also could observe single crystals. The crystals for the mixed alkali metal compounds A₈Tl₁₁X_x happened to form multicrystals together with A₁₅Tl₂₇

and for the reported single crystals (except $K_4Rb_4Tl_{11}Cl_{0.1}$) the data quality was worse compared to $Cs_8Tl_{11}X$ phases. Therefore, the splitting of the alkali metal position could only be observed for $K_4Rb_4Tl_{11}Cl_{0.1}$, for the remaining mixed alkali compounds splitting positions could not be reasonably introduced. In these cases, we only refined the s.o.f. of the halide (see Section 4.3).

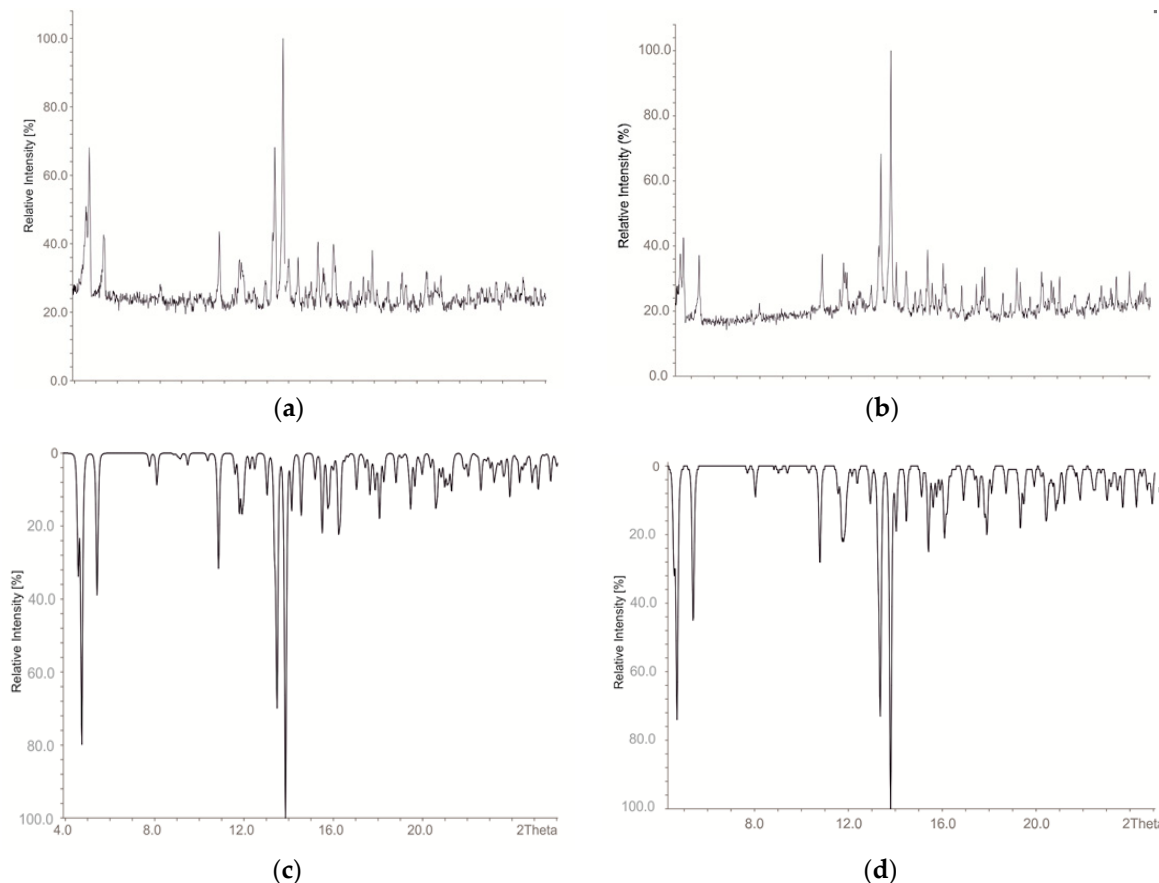


Figure 1. Measured (a) and calculated (c) powder diffraction patterns of $Cs_8Tl_{11}Cl_{0.8}$; Measured (b) and calculated (d) powder diffraction patterns of $Cs_8Tl_{11}Br_{0.9}$ (diffractograms generated by the program STOE WinXPOW [22]).

4. Discussions

4.1. How Does the Geometry of the Thallide Cluster Change on Halide Incorporation?

All A_8Tl_{11} and $A_8Tl_{11}X_x$ compounds include Tl_{11}^{7-} clusters, which are best described as a very compressed, fivefold-capped trigonal prism (Figure 2). Three symmetry independent thallium atoms are located on three different Wyckoff positions of space group $R-3c$: Tl1(12c; 3-fold rotational axis), Tl2(36f; general position) and Tl3(18e; 2-fold rotational axis) build a cluster consisting of 11 Tl atoms with point group D_3 . The deviations from point group D_{3h} are very small and are represented by a distortion of the height of the trigonal prism built by Tl3-atoms. This distortion is also reflected in the distances of Tl2–Tl3 ($d(Tl2-Tl3) = cd$) as there are two crystallographic independent distances present ($d(Tl2-Tl3) = d(Tl2-Tl3\#5)$; $d(Tl3\#3-Tl2) = d(Tl3\#2-Tl2)$). The degree of distortion decreases with increasing similarity of the capping distances (cd).

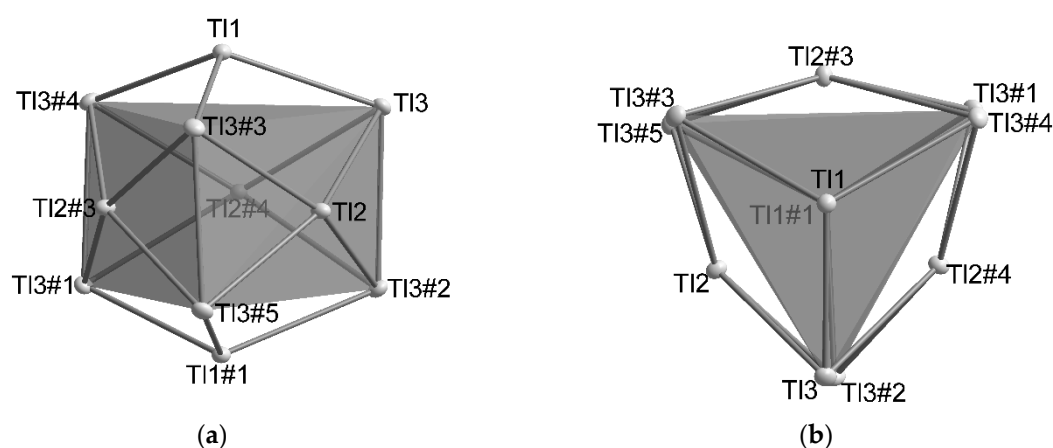


Figure 2. Two perspectives (a) side view; (b) top view show the distortion of the trigonal prism in the Tl_{11}^{7-} cluster which results in the point group D_3 for the cluster; Symmetry operations for the generation of equivalent atoms: #1: $1/3 + x - y, 2/3 - y, 7/6 - z$; #2: $1/3 + y, -1/3 + x, 7/6 - z$; #3: $1 - y, x - y, z$; #4: $1 - x + y, 1 - x, z$; #5: $4/3 - x, 2/3 - x + y, 7/6 - z$.

In Tables 2 and 3 the distances as well as the distortion angles are listed and the dependence on the amount of halide incorporation is clearly evident. In contrast, the height of the trigonal prism (Tl3–Tl3) as well as the distance of the capping atom Tl2 to the mean plane built by Tl3 atoms [$d(Tl2\text{-plane}) = 0.5 \text{ \AA}$ in all compounds] do not significantly change. Based on these observations we introduced a cdd/cd_{av} ratio (cdd : capping distance difference; cd_{av} : average capping distance; (Equation (1)) which allowed for a quick estimation of the degree of distortion. The dependence of the cdd/cd_{av} ratio on the amount of halide is conspicuous and therefore allows for the evaluation of the involvement of halide atoms by solely analyzing the distances between heavy atom positions.

Table 2. Selected distances in \AA (numbering scheme according to, values taken from [1,15]), tilt angle and cdd/cd_{av} value for K_8Tl_{11} and Rb_8Tl_{11} .

Atom 1	Atom 2	K_8Tl_{11}	Rb_8Tl_{11}
Tl2	Tl3	3.0476 (4)	3.060
Tl2	Tl3 ³	3.1396 (4)	3.157
Tl1	Tl3 ¹	3.1304 (4)	3.147
Tl3	Tl3 ³	3.2054 (7)	3.219
Tilt [$^\circ$]		4.69 (2)	4.90
cdd/cd_{av} [%]		2.97	3.12

Table 3. Selected distances in \AA (numbering scheme according to), tilt angle and cdd/cd_{av} value for $Cs_8Tl_{11}Cl_{0.8}$, $Cs_8Tl_{11}Br_{0.9}$, $Cs_5Rb_3Tl_{11}Cl_{0.5}$ and $Cs_{5.7}K_{2.3}Tl_{11}Cl_{0.6}$ and $K_4Rb_4Tl_{11}Cl_{0.1}$.

Atom 1	Atom 2	$Cs_8Tl_{11}Cl_{0.8}$	$Cs_8Tl_{11}Br_{0.9}$	$Cs_5Rb_3Tl_{11}Cl_{0.5}$	$Cs_{5.7}K_{2.3}Tl_{11}Cl_{0.6}$	$K_4Rb_4Tl_{11}Cl_{0.1}$
Tl2	Tl3	3.0656 (4)	3.0743 (2)	3.0605 (6)	3.0554 (7)	3.0564 (2)
Tl2	Tl3 ³	3.0632 (4)	3.0766 (2)	3.0896 (6)	3.0656 (4)	3.1298 (3)
Tl1	Tl3 ¹	3.0894 (4)	3.1006 (2)	3.1049 (7)	3.0884 (8)	3.1274 (3)
Tl3	Tl3 ³	3.2019 (11)	3.2102 (4)	3.2025 (11)	3.1873 (11)	3.2104 (4)
Tilt [$^\circ$]		0.12 (2)	0.069 (7)	0.94 (2)	0.34 (5)	2.352 (7)
cdd/cd_{av} [%]		0.08	0.07	0.95	0.32	2.38

$$\frac{cdd}{cd_{av}} = \frac{|cd_2 - cd_1|}{\left(\frac{cd_2 + cd_1}{2}\right)}; cd_1 \leq cd_2 \quad (1)$$

4.2. Is There a $Rb_8Tl_{11}Cl$?

Despite numerous efforts we did not succeed in producing crystals of $Rb_8Tl_{11}Cl$ of sufficient quality for a reliable determination of halide incorporation directly from the electron density maps. The incorporation of halide cannot be completely ruled out at this point as there is some residual electron density at Wyckoff position $6b$ according to the position of the halide atom in the previously discussed compounds. The s.o.f. for a chlorine atom at this position refined to a value of 0.08. However, the cdd/cd_{av} ratio of 2.4% compared to 3.0% (K_8Tl_{11}) and 3.1% (Rb_8Tl_{11}) and a tilt angle of 2.4° (K_8Tl_{11} : 4.7° , Rb_8Tl_{11} : 4.9°) are very similar to the values found in $K_4Rb_4Tl_{11}Cl_{0.1}$ and suggest a minimal involvement of chloride. Therefore, we assume that $Rb_8Tl_{11}Cl$ does exist, but the amount of incorporated chlorine is less than 10%, which also is in line with the stated observations of Corbett et al. from powder diffraction experiments.

4.3. How Do Mixed Cation Sites Affect the Amount of Halide Incorporation?

It needs to be emphasized that for the preparation of all compounds the same stoichiometric approach was employed and the dependence of the amount of halide incorporation on the cesium content is conspicuous. Therefore, the cation positions needed to be examined more in detail. There are two different cation positions in the asymmetric unit corresponding to Wyckoff position $36f$ for A1 and Wyckoff position $12c$ for A2. For $Cs_8Tl_{11}X$ the A2 position showed the previously mentioned splitting. By taking this splitting as well as free s.o.f. values for the halide (later fixed at the s.o.f. value for Cs2A) into account, a significantly improved model could be refined (Figure 3).

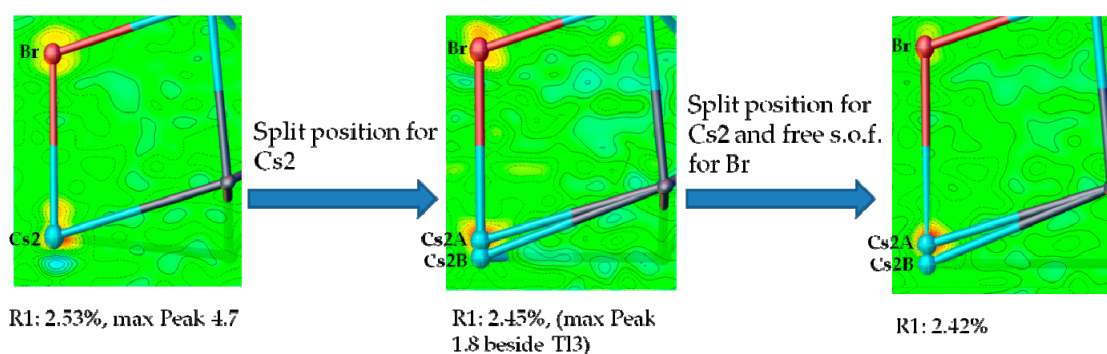


Figure 3. Introduction of split positions and free s.o.f. values for the halide in $Cs_8Tl_{11}Br_{0.9}$ results in an improved model (residual electron density maps, generated by Olex2 [23]).

For $Cs_5Rb_3Tl_{11}Cl_{0.5}$ and $Cs_{5.7}K_{2.3}Tl_{11}Cl_{0.6}$ the position of A1 is mixed occupied by both alkali metals and the s.o.f. values for cesium on the mixed position are very similar to the s.o.f. values of the halide position. The position of A2 is only occupied by the heavier alkali metal cesium, which is in accordance with the observations of Corbett et al. for the binary A_8Tl_{11} phases [14]. In summary, this would mean a favored halide incorporation when cesium is present on both crystallographically independent alkali metal positions. To prove this assumption, we investigated the system K-Rb-Tl in a stoichiometric approach to produce $K_4Rb_4Tl_{11}Cl$ which resulted in crystals of $K_4Rb_4Tl_{11}Cl_{0.1}$ (besides the side products $(K,Rb)_{15}Tl_{27}$ and $(K,Rb)Cl$). Careful investigation of the data of $K_4Rb_4Tl_{11}Cl_{0.1}$ showed the splitting of the A2 position, whereby convergence of the refinement was achieved when A1 and one splitting position are mixed occupied by Rb and K. The second splitting position Rb2A is exclusively occupied by Rb. The overall s.o.f. for A2 was fixed at unity using a SUMP restraint. At the max. peak of the residual electron density a chlorine atom was placed of which the s.o.f. refined at 0.103 (13) and was fixed according to the s.o.f. of Rb2A (Figure 4).

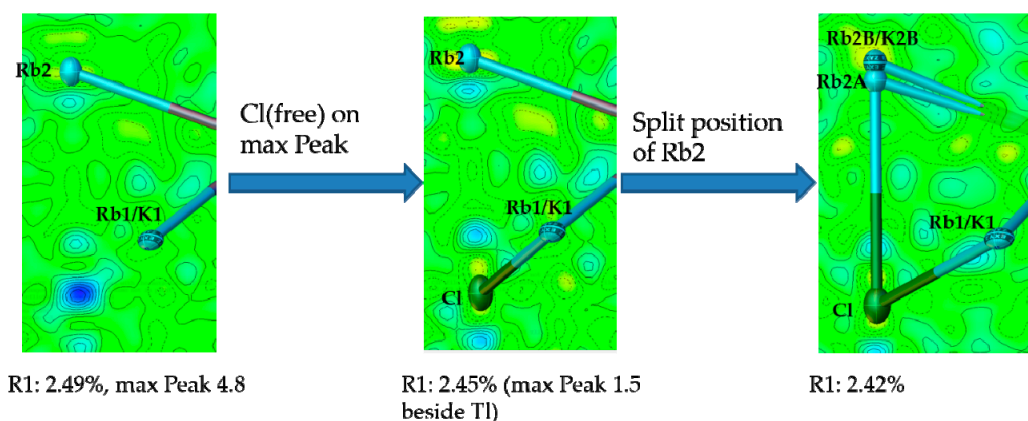


Figure 4. Introduction of split positions and free s.o.f. values for the halide in $K_4Rb_4Tl_{11}Cl_{0.1}$ results in an improved model (residual electron density maps, generated by Olex2 [23]).

The resulting coordination sphere of the halide is best described as distorted cubic, where the longer distances are along the room diagonal of the cubic arrangement from the halide to the position of A2. This distance shortens significantly for X-A2 by introducing split positions (same s.o.f. as halide), resulting in a less distorted cubic arrangement (Figure 5). This cubic arrangement greatly resembles the coordination of the halide in the CsCl structure type ($d(\text{Cs}-\text{Cl}) = 3.573 \text{ \AA}$; $d(\text{Cs}-\text{Br}) = 3.718 \text{ \AA}$). The distances within the distorted cubic arrangements as well as the s.o.f. values for the halide/split position in $\text{Cs}_8\text{Tl}_{11}\text{X}$ ($\text{X} = \text{Cl}$ or Br) and $K_4\text{Rb}_4\text{Tl}_{11}\text{Cl}_{0.1}$ are listed in Tables 4 and 5 lists distances as well as s.o.f. values of the mixed occupied sites within $\text{Cs}_5\text{Rb}_3\text{Tl}_{11}\text{Cl}_{0.5}$ and $\text{Cs}_{5.7}\text{K}_{2.3}\text{Tl}_{11}\text{Cl}_{0.6}$.

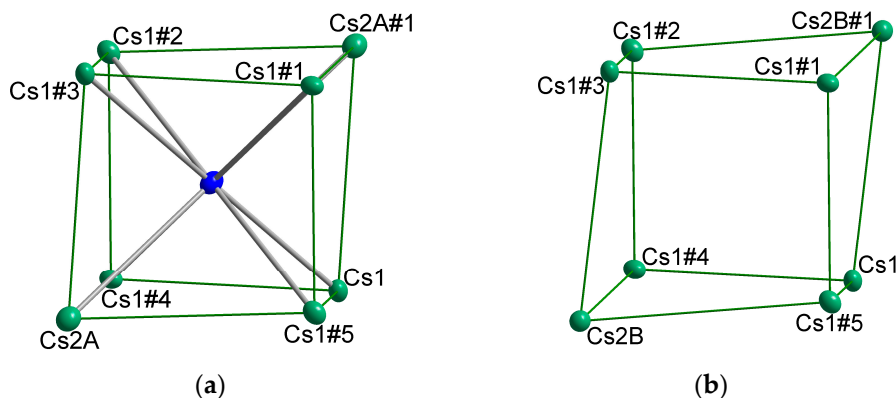


Figure 5. Distorted cubic arrangement around the halide (a); respectively void (b). Cs1: x, y, z ; Cs1#1: $1 - y, x - y, z$; Cs1#2: $1 - x + y, 1 - x, z$; Cs1#3: $4/3 - x, 2/3 - y, 2/3 - z$; Cs1#4: $1/3 + y, 2/3 - x + y, 2/3 - z$; Cs1#5: $1/3 + x - y, -1/3 + x, 2/3 - z$; Cs2A/B: x, y, z ; Cs2A/B#1: $4/3 - x, 2/3 - y, 2/3 - z$.

Table 4. Distances in [\AA] within the distorted cubic arrangement around the halide/void and s.o.f. values for the halide/Cs2A (split position) in $\text{Cs}_8\text{Tl}_{11}\text{X}$ ($\text{X} = \text{Cl}$ or Br) and $K_4\text{Rb}_4\text{Tl}_{11}\text{Cl}_{0.1}$.

Position 1–Position 2	$\text{Cs}_8\text{Tl}_{11}\text{Br}_{0.9}$	$\text{Cs}_8\text{Tl}_{11}\text{Cl}_{0.8}$	Position 1–Position 2	$K_4\text{Rb}_4\text{Tl}_{11}\text{Cl}_{0.1}$
Cs2A-X1	3.990 (2)	3.991 (9)	Rb2A-X1	3.80 (2)
Cs2B-void	4.388	4.354	K2B/Rb2B-void	4.096 (3)
Cs1-X1/void	3.6705 (4)	3.5876 (7)	K1/Rb1-X1/void	3.5994 (9)
s.o.f. (X1/Cs2A)	0.924 (6)	0.76 (2)	s.o.f. (X1/Rb2A)	0.103 (13)

Table 5. Distances in [Å] within the cubic arrangement around the halide/void in $\text{Cs}_5\text{Rb}_3\text{Tl}_{11}\text{Cl}_{0.5}$ and $\text{Cs}_{5.7}\text{K}_{2.3}\text{Tl}_{11}\text{Cl}_{0.6}$. The s.o.f. values for Cs at the mixed occupied A1 site resemble the s.o.f. values for the halide (numbering scheme according to Figure 5).

Position 1–Position 2	$\text{Cs}_5\text{Rb}_3\text{Tl}_{11}\text{Cl}_{0.5}$	$\text{Cs}_{5.7}\text{K}_{2.3}\text{Tl}_{11}\text{Cl}_{0.6}$
A2-X1/void	4.099 (2)	4.002
A1-X1/void	3.6160 (13)	3.5492 (2)
s.o.f. (A1 = Cs)	0.521 (12)	0.612 (9)
s.o.f. (X1)	0.50 (4)	0.60 (4)

The same stoichiometric approach to produce the hitherto presented compounds also was employed by using solely potassium. Here, we only observed well crystallized halide-free K_8Tl_{11} and $\text{K}_{15}\text{Tl}_{27}$ phases. The previously stated stability of the halide including $\text{A}_8\text{Tr}_{11}\text{X}$ phases might not exclusively be caused by the effect of charge balance due to halide incorporation but by the stabilization of a preferably heavier halide atom in a distorted cubic arrangement including cesium preferentially (Figure 6). If less (or no) cesium is involved, then less (or even no) halide will be incorporated. If rubidium is involved as the heaviest alkali metal, then the amount of incorporated halide seems to be limited to approximately 10%. In return, the Tl_{11} clusters themselves seem to tolerate any charge between 7^- and 8^- .

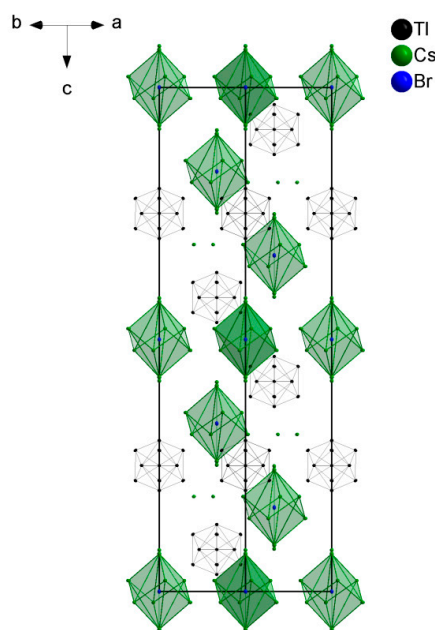


Figure 6. The unit cell of $\text{Cs}_8\text{Tl}_{11}\text{Br}_{0.9}$ shows the two characteristic components: Tl_{11} clusters and the distorted cubic arrangement around the halide atom.

Author Contributions: Conceptualization, S.G.; Methodology, S.G., S.T., B.H., S.S.; Validation, S.G.; Formal Analysis, S.G., S.S., B.H.; Investigation, S.G., S.T.; Resources, N.K.; Writing-Original Draft Preparation, S.G., S.T.; Writing-Review & Editing, S.G.; Visualization, S.G., S.T.; Supervision, S.G.; Project Administration, S.G.

Funding: This work was supported by the German Research Foundation (DFG) within the funding programme Open Access Publishing.

Acknowledgments: The authors thank Marc Schlosser (working group of A. Pfitzner) for collecting the powder diffraction patterns and Dr. Michael Bodensteiner (X-ray Structure department) for discussions concerning the refinement of $(\text{K,Rb})_8\text{Tl}_{11}\text{Cl}_{0.1}$.

Conflicts of Interest: The authors declare no conflict of interest.

Appendix

Stoichiometric approaches

$\text{Cs}_8\text{Tl}_{11}\text{Cl}_{0.8}$: 0.445 g Cs (3.3 mmol), 1.076 g Tl (5.3 mmol Tl) and 0.081 g CsCl (0.51 mmol)

$\text{Cs}_8\text{Tl}_{11}\text{Br}_{0.9}$: 0.413 g Cs (3.1 mmol), 0.998 g Tl (4.9 mmol Tl) and 0.091 g CsBr (0.44 mmol)

$\text{Cs}_5\text{Rb}_3\text{Tl}_{11}\text{Cl}_{0.5}$: 0.246 g Cs (1.9 mmol), 0.128 g Rb (1.5 mmol), 1.124 g Tl (5.5 mmol) and 0.061 g RbCl (0.5 mmol)

$\text{Cs}_{5.7}\text{K}_{2.3}\text{Tl}_{11}\text{Cl}_{0.6}$: 0.264 g Cs (2 mmol), 0.058 g K (1.5 mmol), 1.117 g Tl (5.5 mmol) and 0.037 g KCl (0.5 mmol)

$\text{K}_{3.98}\text{Rb}_{4.02}\text{Tl}_{11}\text{Cl}_{0.1}$: 0.154 g Rb (1.8 mmol), 0.052 g K (1.3 mmol), 1.0134 g Tl (5 mmol) and 0.034 g KCl (0.45 mmol)

References

- Gärtner, S.; Korber, N. Polyanions of group 14 and group 15 elements in alkali and alkaline earth metal solid state compounds and solvate structures. In *Zintl Ions Principles and Recent Developments*, Fässler, T.F., Ed.; Springer: Berlin, Germany, 2011; pp. 25–56.
- Gärtner, S.; Korber, N. Chapter 1.09-Zintl anions. In *Comprehensive Inorganic Chemistry II*, 2nd ed.; Reedijk, J., Poeppelmeier, K., Eds.; Elsevier: Amsterdam, The Netherlands, 2013; pp. 251–267.
- Corbett, J.D. Polyanionic clusters and networks of the early p-element metals in the solid state: Beyond the zintl boundary. *Angew. Chem. Int. Ed.* **2000**, *39*, 670–690. [[CrossRef](#)]
- Scharfe, S.; Kraus, F.; Stegmaier, S.; Schier, A.; Fässler, T.F. Zintl ions, cage compounds, and intermetallic clusters of group 14 and group 15 elements. *Angew. Chem. Int. Ed.* **2011**, *50*, 3630–3670. [[CrossRef](#)] [[PubMed](#)]
- Zintl, E.; Goubeau, J.; Dullenkopf, W. Salzartige Verbindungen und intermetallische Phasen des Natriums in flüssigem Ammoniak. *Z. Phys. Chem.* **1931**, *154*, 1–46. [[CrossRef](#)]
- Zintl, E.; Dullenkopf, W. Über den Gitterbau von NaTl und seine Beziehung zu den Strukturen des β -Messings. *Z. Phys. Chem.* **1932**, *B16*, 195–205. [[CrossRef](#)]
- Eisenmann, B.; Cordier, G. Structural patterns of homo- and heteronuclear anions in zintl phases and related intermetallic compounds and concepts for their interpretation. In *Chemistry, Structure and Bonding of Zintl Phases and Ions*; Kauzlarich, S.M., Ed.; VCH Verlagsgesellschaft mbH: Weinheim, Germany, 1996; pp. 61–137.
- Guloy, A.M. Polar intermetallics and zintl phases along the zintl border. In *Inorganic Chemistry in Focus III*; Wiley-VCH Verlag GmbH & Co.: Weinheim, Germany, 2006.
- Hansen, D.A.; Smith, J.F. Structure and bonding model for Na_2Tl . *Acta Cryst.* **1967**, *22*, 836–845. [[CrossRef](#)]
- Marsh, R.E.; Shoemaker, D.P. The crystal structure of NaPb. *Acta Cryst.* **1953**, 197–205. [[CrossRef](#)]
- Busmann, E. Die kristallstrukturen von KSi, RbSi, KGe, RbGe und CsGe. *Z. Anorg. Allg. Chem.* **1961**, *313*, 90–106. [[CrossRef](#)]
- Lorenz, C.; Gärtner, S.; Korber, N. Ammoniates of zintl phases: Similarities and differences of binary phases A_4E_4 and their corresponding solvates. *Crystals* **2018**, *8*, 276. [[CrossRef](#)]
- Blase, W.; Cordier, G.; Müller, V.; Haussermann, U.; Nesper, R.; Somer, M. Preparation and crystal-structures of $\text{Rb}_8\text{In}_{11}$, K_8Tl_{11} , and $\text{Rb}_8\text{Tl}_{11}$ band-structure calculations on K_8In_{11} . *Z. Naturforsch. B* **1993**, *48*, 754–760. [[CrossRef](#)]
- Dong, Z.-C.; Corbett, J.D. A_8Tl_{11} (A = K, Rb, or Cs) Phases with Hypoelectronic Tl_{11}^{7-} cluster anions: Syntheses, structure, bonding and properties. *J. Cluster Sci.* **1995**, *6*, 187–201. [[CrossRef](#)]
- Dong, Z.C.; Corbett, J.D. $\text{A}_{15}\text{Tl}_{27}$ (A = Rb, Cs): A structural type containing both isolated clusters and condensed layers based on the tl-11 fragment. Syntheses, structure, properties, and band structure. *Inorg. Chem.* **1996**, *35*, 1444–1450. [[CrossRef](#)] [[PubMed](#)]
- Sevov, S.C.; Corbett, J.D. A remarkable hypoelectronic indium cluster in K_8In_{11} . *Inorg. Chem.* **1991**, *30*, 4875–4877. [[CrossRef](#)]
- Wang, F.; Wedig, U.; Prasad, D.; Jansen, M. Deciphering the chemical bonding in anionic thallium clusters. *J. Am. Chem. Soc.* **2012**, *134*, 19884–19894. [[CrossRef](#)] [[PubMed](#)]
- Henning, R.W.; Corbett, J.D. $\text{Cs}_8\text{Ga}_{11}$, a new isolated cluster in a binary gallium compound. A family of valence analogues $\text{A}_8\text{Tr}_{11}\text{X}$: A = Cs, Rb; Tr = Ga, In, Tl; X = Cl, Br, I. *Inorg. Chem.* **1997**, *36*, 6045–6049. [[CrossRef](#)] [[PubMed](#)]

19. Falk, M.; El Addad, A.; Röhr, C. Crystal and electronic structure of alkali triele halogenides of the K_8In_{11} -type structure. In Proceedings of the 25th Annual Conference of the German Crystallographic Society, Karlsruhe, Germany, 27–30 March 2017.
20. Hackspill, L. Sur quelques propriétés des métaux alcalins. *Helv. Chim. Acta* **1928**, *11*, 1003–1026. [[CrossRef](#)]
21. Agilent. *CrysAlis pro. v.39.37b ed.*; Agilent Technologies Ltd.: Yarnton, UK, 2014.
22. *Computer Program: STOE WinXPOW*; STOE & Cie 2000 Darmstadt: Darmstadt, Germany, 2011.
23. Dolomanov, O.V.; Bourhis, L.J.; Gildea, R.J.; Howard, J.A.K.; Puschmann, H. Olex2: A complete structure solution, refinement and analysis program. *J. Appl. Crystallogr.* **2009**, *42*, 339–341. [[CrossRef](#)]



© 2018 by the authors. Licensee MDPI, Basel, Switzerland. This article is an open access article distributed under the terms and conditions of the Creative Commons Attribution (CC BY) license (<http://creativecommons.org/licenses/by/4.0/>).